Microstructure characterization and cation distribution of nanocrystalline magnesium ferrite prepared by ball milling

S.K. Pradhan [a,b,*], S. Bid [b], M. Gateshki [a], V. Petkov [a]

[a] *Department of Physics, 203, Dow Science, Central Michigan University, MI 48859, USA*
[b] *Department of Physics, The University of Burdwan, Golapbag, Burdwan 713104, West Bengal, India*

Abstract

Nanocrystalline magnesium ferrite is synthesized by high-energy ball milling. The formation of nanocrystalline ferrite phase is observed after 3 h of milling and its content increases with milling time. The structural and microstructural evolution of the nanophase have been studied by X-ray powder diffraction and the Rietveld method. After 3 h of milling, ferrite phase (mixed spinel) nucleates from the starting α-Fe_2O_3–MgO solid solution. After 5 h of milling, a second ferrite phase (inverse spinel) with a larger lattice parameter emerges and its content grows in parallel with that of the mixed spinel matrix. After 11 h of milling, only a very small amount ($\sim$3 wt.%) of the starting α-Fe_2O_3 remains unused. With increasing milling time the type of the cationic distribution over the tetrahedral and octahedral sites in the lattice of the nanocrystalline material changes from a mixed to inverse type. Microstructure characterization by HRTEM corroborates the findings of X-ray analysis.
© 2005 Elsevier B.V. All rights reserved.

Keywords: Nanocrystalline Mg-ferrite; Ball milling; Cation distribution; Microstructure; Rietveld method

1. Introduction

Nanocrystalline spinel ferrites have been investigated intensively in recent years due to their potential applications in non-resonant devices, radio frequency circuits, high-quality filters, rod antennas, transformer cores, read/write heads for high-speed digital tapes and operating devices [1–6]. Magnesium ferrite, $MgFe_2O_4$, is a soft magnetic n-type semiconducting material [7], which finds a number of applications in heterogeneous catalysis, adsorption, sensors and in magnetic technologies. High-energy ball milling is a solid-state processing technique very suitable for the preparation of nanocrystalline ferrite powders exhibiting many of the useful properties listed above [8–11]. However, reports on preparation of nanocrystalline Mg-ferrites by high-energy ball milling of a mixture of MgO and α-Fe_2O_3 are not found in the literature. To the best of our knowledge, so far the

microstructure, phase transformation kinetics and cation distributions in ball mill prepared Mg-ferrites have not been studied in details either. Here, we report the results of such a study.

Ferrites have the general formula $(M_{1-x}Fe_x)$ $[M_xFe_{2-x}]O_4$. The divalent metal element M (Mg, Zn, Mn, Fe, Co, Ni or mixture of them) can occupy either tetrahedral (A) or octahedral [B] sites in the cubic, spinel-type structure. The structural formula of Mg-ferrite is usually written as $(Mg_{1-x}Fe_x)[Mg_xFe_{2-x}]O_4$, where x represents the degree of inversion (defined as the fraction of (A) sites occupied by Fe^{3+} cations). The magnetic properties of a spinel ferrite are strongly dependent on the distribution of the different cations among (A) and [B] sites. The cation distribution of a slowly cooled Mg-ferrite (from 1773 K to room temperature) was reported [12–14] as nearly inverse with $x = 0.9$ (cubic, $a = 0.83998$ nm, space group: $Fd\bar{3}m$, $Z = 8$; ICDD PDF #88–1943). It has been also experimentally verified that the distribution of cations among the lattice sites depends on material's preparation. This often leads

* Corresponding author. Tel.: +91 342 2557282; fax: +91 342 2530452.
 E-mail address: skpdn@vsnl.net (S.K. Pradhan).

to a variation in the unit cell dimensions. Both variations are seen as broadening and/or shift of the diffraction lines. As the ionic radii of Mg^{2+} and Fe^{3+} are quite different, different distributions of cations will also lead to different lattice strain. All these effects may be accounted for by analysis of the profiles of the peaks in the powder diffraction pattern.

During ball milling, materials suffer severe high-energy impacts through ball-to-ball and ball-to-vial-wall collisions. Formation of the nanocrystalline product results from fragmentation and re-welding of crystalline grains. These two processes are known to produce a considerable amount of structural and microstructural defects. Physical properties of materials depend upon their microstructure and, therefore, its knowledge is an important prerequisite to controlling material's performance. Rietveld analysis [15–17] has been adopted in the present study to determine the microstructural parameters of nanocrystalline $MgFe_2O_4$. The analysis aims at: (i) studying the phase transformation kinetics of the ball milling process; (ii) determining the relative phase abundances of the product at different stages of the process; (iii) characterizing the prepared materials in terms of microstructural parameters such as crystallite size and root mean square (r.m.s.) lattice strain and (iv) estimating the distribution of cations among (A) and [B] sites in the spinel lattice.

2. Experimental

Accurately weighed powders of 20.15 wt.% MgO (Merck, 99% purity) and 79.85 wt.% of α-Fe_2O_3 (Glaxo, 99% purity) were hand-ground in an agate mortar under doubly distilled acetone for more than 5 h. High-energy ball milling of the homogeneous powder mixture was carried out with a planetary ball mill (Model P5; Fritsch GmbH, Germany). Milling was done at room temperature in a hardened chrome steel (Fe–1 wt.% Cr) vial (volume 80 ml) using 30 hardened chrome steel balls of 10 mm diameter at ball to powder mass ratio (BPMR) = 40:1. The rotation speed of the disk was 325 rpm and that of the vial ~475 rpm. The time of milling was varied from 1 to 11 h depending upon the progress of formation of Mg-ferrite phase.

The X-ray powder diffraction patterns of the starting mixture and ball-milled samples were collected on a Philips X'Pert powder diffractometer using Cu Kα radiation. The background scattering and fluorescent radiation were reduced by employing a diffracted beam graphite monochromator and 0.5° anti-scattering slit. The X-ray beam was collimated using 0.5° divergence slit. The diffracted intensities were collected in step-scan mode (step size $2\theta = 0.02°$; counting time 10–60 s) in the angular range $2\theta = 15$–100°. To correct instrumental broadening a Si standard [22] was used. Microstructure characterization of 9 h ball milled powder has also been done using HRTEM (Model GEM 2010, JEOL, Japan) at 200 kV.

3. Rietveld analysis of the experimental data

3.1. Method of analysis

In the Rietveld analysis, we employed the program MAUDWEB 1.9992 [17]. It is designed to refine simultaneously both the structural (lattice cell constants and atomic positions and occupancies) and microstructural parameters (crystallite size and r.m.s. strain). The shape of the peaks in the experimental diffraction patterns was well described by an asymmetric pseudo-Voigt (pV) function. The background of each pattern was fitted by a polynomial function of degree 5. To simulate the theoretical X-ray powder diffraction patterns of MgO, α-Fe_2O_3, Mg-ferrite (normal spinel) and Mg-ferrite (inverse spinel) the following considerations for the different phases were made:

(i) MgO (cubic, space group: $Fm\bar{3}m(225)$, $a = 0.42$ nm (ICDD PDF # 87-0653)), Mg^{2+} and O^{2-} in special Wyckoff positions $4a$ and $4b$, respectively;

(ii) α-Fe_2O_3 (rhombohedral, space group: $R\bar{3}c(167)$, $a = 0.5032$ and $c = 1.3733$ nm (ICDD PDF # 89-0599)) with Fe and O atoms in special Wyckoff positions $12c$ and $18e$, respectively;

(iii) Mg-ferrite (cubic, space group: $Fd\bar{3}m(227)$, $a = 0.83998$ nm (ICDD PDF # 88-1943)) with Mg^{2+} (A-site), Fe^{3+} [B-site] for normal spinel and with 0.1 $Mg^{2+} + 0.9 Fe^{3+}$ (A-site), 0.5 $Mg^{2+} + 0.5 Fe^{3+}$ [B-site]. Wyckoff positions for (A) site, [B] site, and O^{2-} are $8a$, $16d$ and $32e$, respectively.

3.2. Crystal structure refinement

A detailed account of the mathematical procedures implemented in the Rietveld analysis has been reported elsewhere [15–21]. Here, we give a brief, step-by-step description of the analysis of the experimental powder diffraction patterns done by us. First, the positions of the peaks were corrected for zero-shift error by successive refinements. Considering the integrated intensity of the peaks to be a function of the refined structural parameters, the Marquardt least-squares procedure was adopted for minimizing the difference between the observed and simulated powder diffraction patterns. The progress of the minimization was monitored through the usual reliability parameters, R_{wp} (weighted residual factor), and R_{exp} (expected residual factor) defined as

$$R_{wp} = \left[\frac{\sum_i w_i (I_0 - I_c)^2}{\sum_i w_i (I_0)^2} \right]^{1/2}$$

$$R_{exp} = \left[\frac{N - P}{\sum_i w_i (I_0)^2} \right]^{1/2}$$

where I_0 and I_c are the experimental and calculated intensities, $w_i = 1/I_0$ are weight factors, N is the number of experimental observations and P is the number of refined

parameters. Also, we used the so-called goodness of fit (GoF) factor [17–21]:

$$GoF = \frac{R_{wp}}{R_{exp}}$$

Refinements were carried out until convergence was reached and the value of the GoF factor became close to 1 (usually, the final GoF varies from 1.1 to 1.3). There is a simple relationship [18–21] between the individual scale factor determined of a crystalline phase in a multiphase material, and the phase concentration (weight fraction) in the mixture. We used it to obtain the weight fraction (W_i) for each phase as follows:

$$W_i = \frac{S_i(ZMV)_i}{\sum_j S_j(ZMV)_j}$$

where S_j is the refined scale factor of phase i, Z the number of formula units per unit cell, M the atomic weight of the formula unit and V is the volume of the unit cell.

3.3. Size-strain analysis

It has been well established that the observed broadening of the diffraction peaks is mainly due to small crystallite size and the presence of root mean square (r.m.s.) strain inside the crystallites. The crystallite size and strain broadening can be approximated with Cauchy and Gaussian type functions, respectively [18–22]. Thus, the basic consideration of the method employed in the Rietveld analysis and by us is the modeling of the diffraction profiles with an analytical function, which is a combination of Cauchy and Gauss as well as a function taking into account the asymmetry in the diffraction profile. Again, the process of successive profile refinements was adopted to refine the crystallite size and strain in the studied materials. The refinement was continued until

convergence was reached and the value of the quality factor (GoF) approached 1.

4. Results and discussion

The XRD powder patterns from unmilled homogeneous mixture of MgO and α-Fe$_2$O$_3$ and ball-milled samples are shown in Fig. 1. The powder pattern of the unmilled mixture shows the individual reflections of MgO and α-Fe$_2$O$_3$ phases. MgO reflections are very weak (20.15 wt.%) when compared to those of α-Fe$_2$O$_3$ (79.15 wt.%). As can be seen in the figure, Mg-ferrite is formed after just 3 h of milling. Mg-ferrite phase manifests itself through its strongest (2 2 0) ($2\theta \approx 30.2°$) and (3 1 1) (partially overlapped, $2\theta \approx 35.4°$) Bragg peaks. Its amount increases gradually with increasing milling time. With the progress of milling, more Bragg peaks of the ferrite phase appear. The peaks are, however, fairly broad and asymmetric as it is expected to be with a nanocrystalline material. A critical comparison between the ball-milled nanocrystalline ferrite and ICDD reported bulk Mg-ferrite phases reveals that there are anomalies in the intensity distribution of some peaks. As the bulk Mg-ferrite is nearly inverse spinel, this anomaly in the intensity distribution may arise from the following effects: (i) differences in the cation distribution among the (A) and [B] sites in the spinel lattice and (ii) phase inhomogeneity, in particular, a presence of ferrite phases with different cation distributions. The differences in the intensity distribution were taken into account by considering an additional ferrite phase with a somewhat larger lattice parameter and with a different cation distribution (Fig. 2). The refinement result showed that the major nanocrystalline ferrite phase is a mixed spinel while the additional minor nanocrystalline phase with larger lattice parameter is nearly an inverse spinel. It is interesting
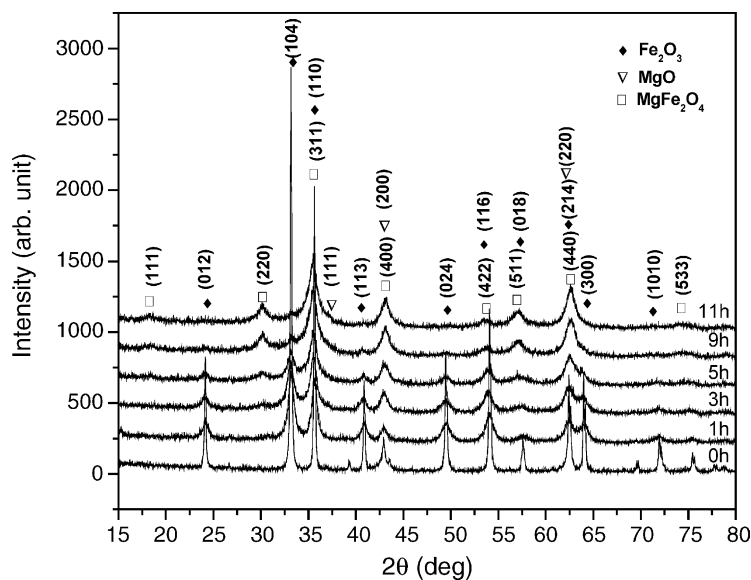

Fig. 1. X-ray powder diffraction patterns of unmilled (0 h) (1:1 mol%) and ball milled MgO–α-Fe$_2$O$_3$ mixture for different time intervals.
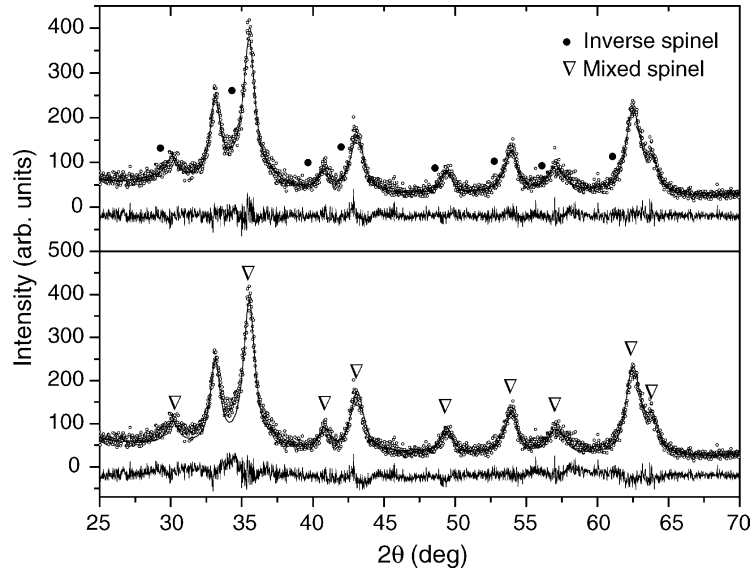
Fig. 2. Powder diffraction patterns (symbols) and Rietveld refinement results (line) for nanocrystalline Mg ferrite after 5 h milling. The positions of inverse spinel reflections at the low-angle side of the mixed spinel reflections are marked with solid points. The quality of fitting improves (upper) by taking into account the presence of a minor inverse spinel phase. The unmarked peak belongs to α-Fe_2O_3.
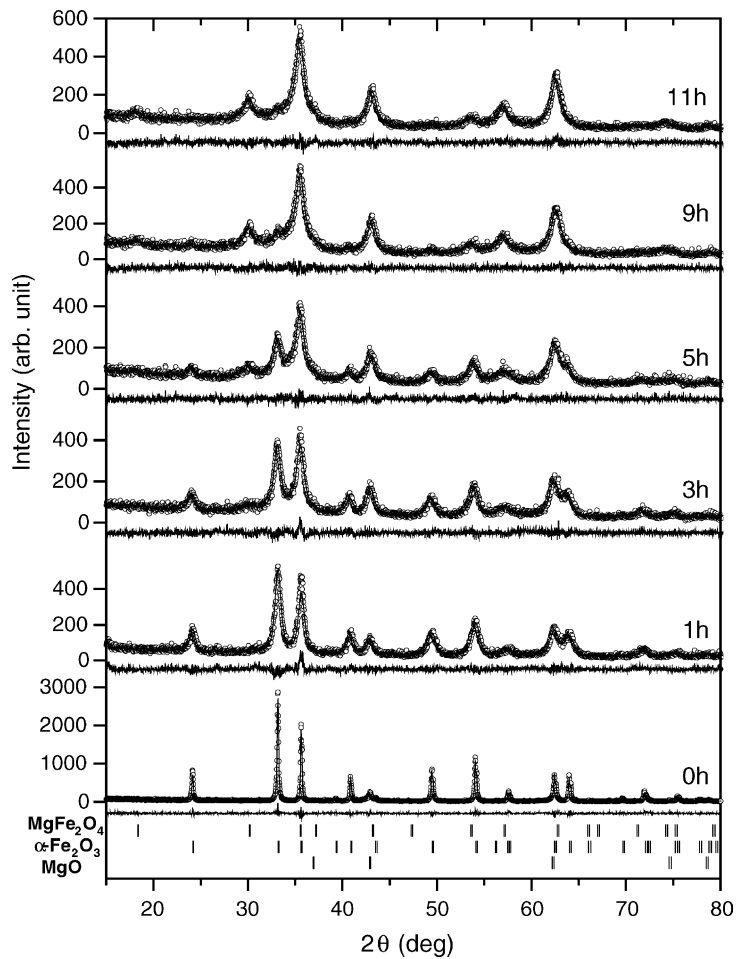

Fig. 3. Observed (symbol) and calculated (line) X-ray powder diffraction patterns of ball milled MgO–α-Fe_2O_3 mixture for different periods of milling time. Peak positions of the different phases are shown at the base line as small bars.

to note that the peak-broadening of nanocrystalline ferrite reflections depends on $(h\,k\,l)$ and not on the angle of scattering. In particular, the higher order reflection $(4\,4\,0)$ appears with less peak-broadening than the low order $(2\,2\,0)$, see Figs. 1 and 2. This made it difficult to fit all reflections with a single angle-dependent peak-broadening model. The quality of profile fitting did not improve even with peak-asymmetry refinement. It, however, improved significantly by taking into account the peak-asymmetry at the base of low-angle side of all ferrite reflections as due to another ferrite phase (Fig. 2). Finally, GoF values of all samples were as shown below:

Milling time (h)	R_{wp}	R_{exp}	GoF
1	0.153	0.130	1.173
3	0.143	0.123	1.160
5	0.145	0.126	1.148
9	0.138	0.125	1.096
11	0.132	0.120	1.100

We have obtained similar result when used FULLPROF Rietveld software [23] as well. The presence of two nanocrystalline phases with slightly different lattice parameters and cation distributions is one possible explanation for the observed mismatch between the calculated and experimental intensities (Fig. 2). Another possible reason is the presence of lattice strain originating from a random distribution of cations and/or Fe^{3+} cation deficiency. Considering the above-mentioned effects, all the profiles have been fitted with the Rietveld technique as shown in Fig. 3.

Fig. 4 shows the dependence of relative phase abundances with milling time. The content (wt.%) of MgO phase decreases rapidly and becomes negligible after 3 h of milling. That of α-Fe_2O_3 increases relatively (79.15–84 wt.%) after 1 h of milling and then decreases very fast to ~18 wt.% within 5 h of milling. The initial increase in the phase content
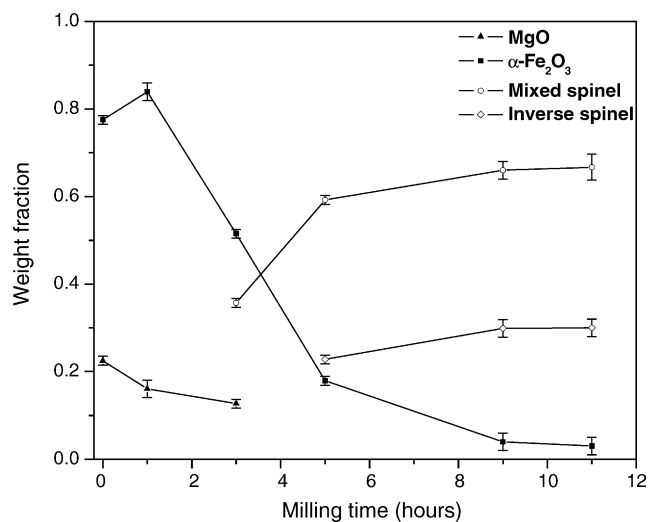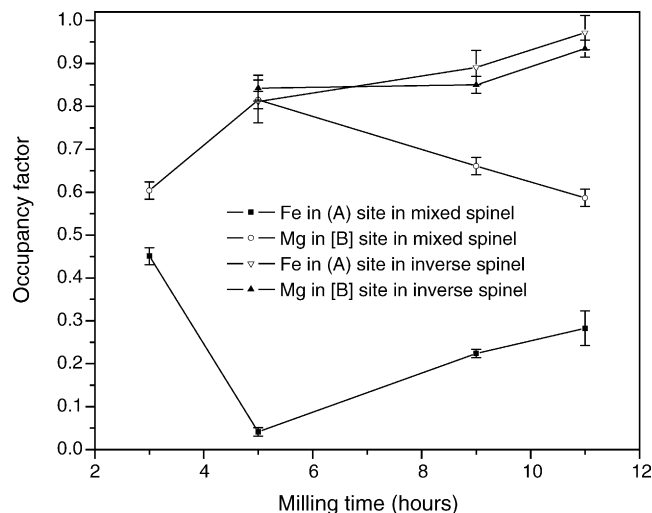

Fig. 5. Variation of cation distribution among (A) and [B] sites in the spinel lattice with milling time.

of α-Fe_2O_3 may be due to the formation of MgO–α-Fe_2O_3 solid solution. The sudden decrease—to the formation of Mg-ferrite phase. After 3 h of milling, a significant amount (~36 wt.%) of Mg-ferrite phase with mixed spinel lattice is formed. Its phase content increases fast to ~59 wt.% within 5 h of milling and then increases slowly to ~67 wt.% after 11 h of milling. The formation of Mg-ferrite with nearly inverse spinel lattice is noticed after 5 h of milling when the phase content of MgO becomes undetectable. It seems that the inverse spinel phase is initiated from the mixed spinel phase due to a solid-state diffusion of nanocrystalline α-Fe_2O_3 into the mixed spinel lattice. The content of this phase increases slowly with milling time. The formation of inverse spinel from mixed one is corroborated by the finding of Harrison and Putnis [24] who studied the time–temperature dependence of magnetic susceptibility of Mg-ferrite. They reported that the cation ordering in Mg-ferrite proceeds via a heterogeneous mechanism, involving nucleation and growth

Fig. 4. Variation of the phase content with milling time as obtained by the present Rietveld refinements.
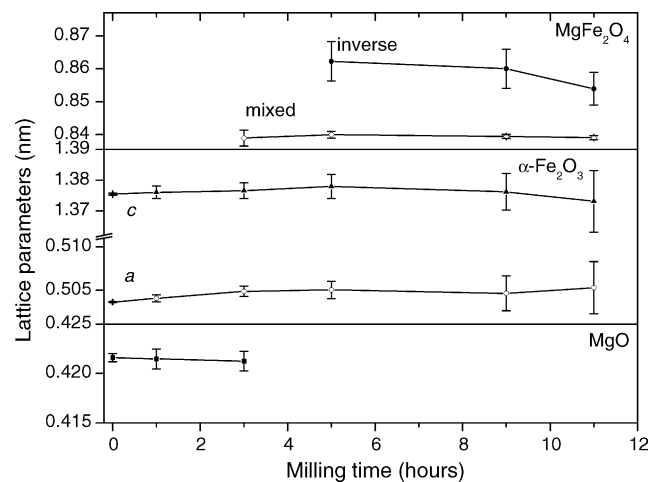

Fig. 6. Variation of lattice parameters of the different phases observed during the milling process as a function of milling time.
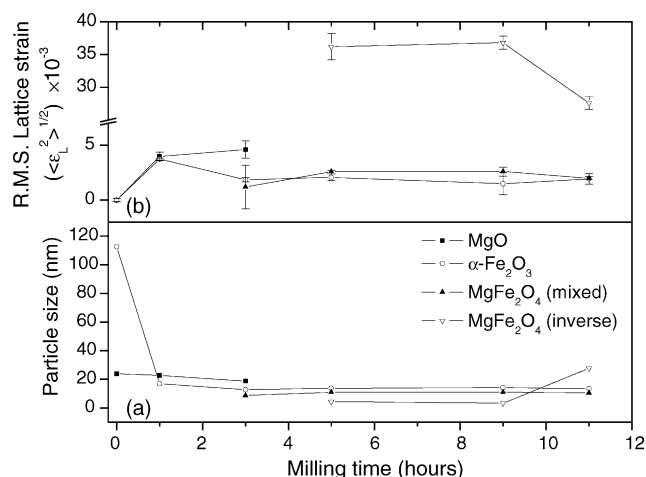
Fig. 7. Variation of (a) crystallite size and (b) r.m.s. lattice strain of the different phases with milling time.

of fine-scale domains of the ordered phase within the matrix of the disordered one.

The formation of mixed spinel instead of inverse spinel at the initial stage of milling may result from an Fe^{3+} cation deficiency due to the fact that after 3 h of milling ∼52 wt.% of α-Fe_2O_3 remains unused. It is interesting to note that during the formation of inverse spinel inside the mixed spinel matrix, the occupancy of Fe^{3+} cation on (A) site becomes very close to normal and then increases with milling time. At the same time, the occupancy of Mg^{2+} cation on [B] site increases and then decreases with milling time (see Fig. 5). This observation suggests that at the later stages of the milling process an inverse spinel phase is formed. This occurs when the random distribution of cations among the (A) and [B] sites inside the mixed spinel matrix becomes similar to that of an inverse spinel ferrite leading to further Fe^{3+} deficiency in the mixed spinel matrix. Up to 11 h of milling, no change is observed in the occupancy factors of cations in the inverse spinel phase. The cation distribution in the mixed spinel proceeds towards the inverse spinel with milling time. This is due to a solid-state diffusion of nanocrystalline α-Fe_2O_3 into the mixed spinel matrix. As the compositions of these two ferrite phases are different, they also have different lattice parameters.

The variation of lattice parameters of the different phases with milling time is shown in Fig. 6. The lattice parameter of cubic MgO decreases insignificantly with milling time. A possible reason is the presence of compressive stress introduced by the ball milling. Both a and c lattice parameters of α-Fe_2O_3 increase linearly with milling time obeying Vegard's law. The increase in lattice parameters is due to substitution of Fe^{3+} (ionic radius = 0.049 nm) by the larger Mg^{2+} (ionic radius = 0.057 nm) ions [25]. The linear dependence acknowledges the formation of MgO–α-Fe_2O_3 solid solution at the early stages of the milling process. After 5 h of milling, a remains nearly constant and c decreases towards the lattice parameter of the unmilled sample. This indicates that the substitution of Fe^{3+} by Mg^{2+} ions occurs preferably
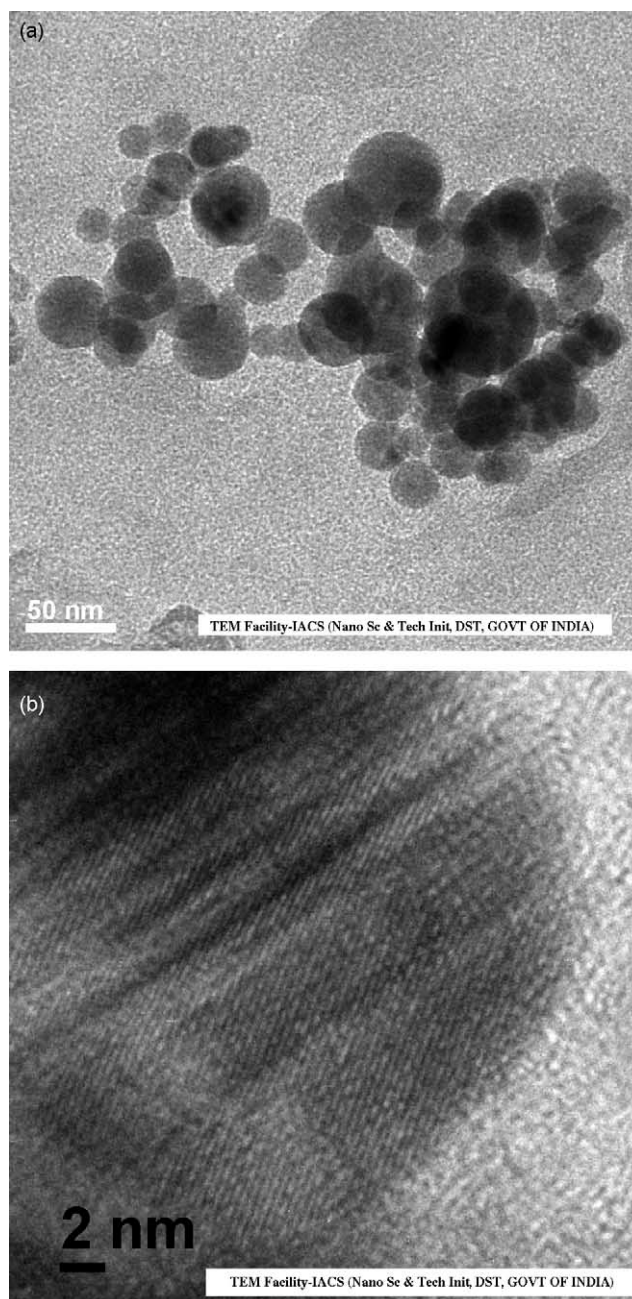

Fig. 8. HRTEM micrographs of 9 h ball milled sample (a) size and shape of Mg-ferrite grains (b). Lattice imaging at the ferrite grain-boundary.

along the c-axis of the unit cell. The lattice parameter of the cubic mixed spinel does not change significantly with milling time. That of the inverse spinel approaches the reported in the literature values. This may be attributed to the release of lattice strain when the host mixed spinel matrix approaches that of the inverse spinel ferrite.

Figs. 1 and 3 show that the diffraction peaks get broader with milling time. This leads to a severe peak overlap. The peak broadening is likely due to both small crystallite size and lattice strain. The crystallite size (coherently diffracting domains) and r.m.s. lattice strain values for the individual

phases have been estimated from the Rietveld refinement and plotted in Fig. 7a and b, respectively. As can be seen in Fig. 7a, the initial crystallite size of α-Fe$_2$O$_3$ is $\sim$115 nm and that of MgO is $\sim$24 nm. After 1 h of milling, the crystallite size of both phases become almost equal. For longer milling times no significant change in the crystallite sizes of both phases is observed. The mixed spinel matrix is formed after 3 h of milling from the MgO–α-Fe$_2$O$_3$ solid solution. It has crystallite size ($\sim$11 nm) slightly smaller than that of the soild-solution phase ($\sim$14 nm). Those crystallite sizes remain almost constant with milling time. The nearly inverse spinel ferrite phase is formed after 5 h of milling inside the mixed spinel matrix. It is characterized with a very small crystallite size ($\sim$4 nm). A significant increase in the crystallite size (from $\sim$4 to $\sim$27 nm) is observed after 11 h of milling. The increase may be considered as crystallite size growth of the inverse spinel phase. As can be seen in Fig. 7b, the r.m.s. strain does not follow any particular pattern.

Microstructure of the 9 h ball-milled sample has also been characterized by HRTEM. TEM micrograph (Fig. 8a) reveals that the grains of ball-milled sample are spherical in shape and average size of the grain is $\sim$25 nm which is quite closer to the X-ray crystallite size (Fig. 7a). However, some of the particles are quite bigger due to agglomeration of small grains and variation in density of grains clearly corroborates the findings. Lattice imaging at the interface of the grains and the so-called background reveals that the lattices inside the grain are almost equally spaced but there are some mistakes along any lattice row (Fig. 8b). It signifies the presence of significant amount of lattice imperfections in the ferrite lattice, which results in peak-broadening. It is interesting to note that there is no such lattice pattern in the background portion of the HRTEM micrograph. It indicates that the minor ferrite phase is almost an amorphous phase, which agrees well with the X-rays results.

5. Conclusions

Nanocrystalline Mg-ferrite was prepared by high-energy ball milling of stoichiometric mixture of MgO and α-Fe$_2$O$_3$ powders. The starting material and the products at different stages of the milling process were characterized by Rietveld analysis of the X-ray powder diffraction patterns. The results of the analyses may be summarized as follows:

(i) Nanocrystalline Mg-ferrite (mixed spinel) is formed within 3 h of milling.
(ii) Nanocrystalline Mg-ferrite with a nearly inverse spinel lattice is formed after 5 h of milling. After 11 h of milling the nanocryslline material contains a mixed spinel as the major phase.
(iii) The occupancy of Fe^{3+} on (A) site (inverse spinel) increases with milling time.
(iv) At the initial stage of ball milling, a mixed spinel phase emerges from the MgO–α-Fe$_2$O$_3$ solid solution. The nearly inverse spinel phase is assumed to grow inside the mixed spinel matrix.
(v) The final product of the milling process is a mixture of inversed and mixed nanocrystalline spinels. Presence of a small amount ($\sim$3 wt.%) of α-Fe$_2$O$_3$ indicates that both ferrite phases are non-stoichiometric in composition. The present study shows that nanocrystalline stoichiometric nearly inverse Mg-ferrite spinel may not be formed completely just by ball-milling the stoichiometric mixture of MgO and α-Fe$_2$O$_3$.
(vi) Microstructure characterization by HRTEM corroborates the findings of X-ray analysis.

References

[1] P. Ravindernathan, K.C. Patil, J. Mater. Sci. 22 (1987) 3261.
[2] H. Igarash, K. Ohazaki, J. Am. Ceram. Soc. 60 (1997) 51.
[3] A. Goldman, Am. Ceram. Soc. Bull. 63 (1984) 582.
[4] D. Stoppels, J. Magn. Magn. Mater. 160 (1996) 323.
[5] K.H. Lee, D.H. Cho, S.S. Jeung, J. Mater. Sci. Lett. 16 (1997) 83.
[6] C.S. Kim, Y.S. Yi, K.T. Park, H. Namgung, J.G. Lee, J. Appl. Phys. 85 (1999) 5223.
[7] R.J. Willey, P. Noirclerc, G. Busca, Chem. Eng. Commun. 123 (1993) 1.
[8] P. Druska, U. Steinike, V. Sepelak, J. Solid State Chem. 146 (1999) 13.
[9] V. Sepelak, A.Yu. Rogachev, U. Steinike, D.Chr. Uccker, S. Wibmann, K.D. Becker, Acta Crystallogr. A 52 (Suppl.) (1996) 367.
[10] V. Sepelak, K. Tkacova, V.V. Boldyrev, U. Steinike, Mater. Sci. Forum 783 (1996) 228.
[11] V. Sepelak, A.Yu. Rogachev, U. Steinike, D.Chr. Uccker, F. Krumcich, S. Wibmann, K.D. Becker, Mater. Sci. Forum 139 (1997) 235.
[12] N.W. Grimes, R.J. Hilleard, J. Waters, J. Yerkess, J. Phys. C (Prog. Phys. Soc.) 1 (1968) 663.
[13] G. Blasse, Philips Res. Rep. Suppl. 3 (1964) 91.
[14] G.E. Bacon, F.F. Roberts, Acta Crystallogr. 6 (1953) 57.
[15] H.M. Rietveld, Acta Crystallogr. 22 (1967) 151.
[16] H.M. Rietveld, J. Appl. Crystallogr. 2 (1969) 65.
[17] L. Lutterotti, MAUDWEB, Version 1.9992, 2004. http://www.ing.unitn.it/~luttero/maud.
[18] S. Bid, S.K. Pradhan, J. Appl. Crystallogr. 35 (2002) 517.
[19] S. Bid, S.K. Pradhan, Mater. Chem. Phys. 82 (2003) 27.
[20] H. Dutta, S.K. Manik, S.K. Pradhan, J. Appl. Crystallogr. 36 (2003) 260.
[21] S.K. Manik, S.K. Pradhan, Mater. Chem. Phys. 86 (2004) 284.
[22] J.G.M. Van Berkum, Ph.D. Thesis, Delft University of Technology, The Netherlands, 1994.
[23] J. Rodriguez-Carvajal, Physica B 192 (1993) 55.
[24] R.J. Harrison, A. Putnis, Phys. Chem. Minerals 26 (1994) 322.
[25] R.D. Shannon, Acta Crystallogr. A 32 (1976) 751.